

Conversion of the stacking orientation of bilayer graphene due to the interaction of BN-dopants

Nzar Rauf Abdullah^{a,b}, Hunar Omar Rashid^a, Chi-Shung Tang^c, Andrei Manolescu^d, Vidar Gudmundsson^e

^aDivision of Computational Nanoscience, Physics Department, College of Science, University of Sulaimani, Sulaimani 46001, Kurdistan Region, Iraq

^bComputer Engineering Department, College of Engineering, Komar University of Science and Technology, Sulaimani 46001, Kurdistan Region, Iraq

^cDepartment of Mechanical Engineering, National United University, 1, Lienda, Miaoli 36003, Taiwan

^dReykjavik University, Department of Engineering, Menntavegur 1, IS-102 Reykjavik, Iceland

^eScience Institute, University of Iceland, Dunhaga 3, IS-107 Reykjavik, Iceland

arXiv:2101.00462v1 [cond-mat.mes-hall] 2 Jan 2021

Abstract

A conversion of AA- to AB-stacking bilayer graphene (BLG) due to interlayer interaction is demonstrated. Two types of interlayer interactions, an attractive and a repulsive, between the Boron and Nitrogen dopant atoms in BLG are found. In the presence of the attractive interaction, an AA-stacking of BN-codoped BLG is formed with a less stable structure leading to weak mechanical properties of the system. Low values of the Young modulus, the ultimate strength and stress, and the fracture strength are observed comparing to a pure BLG. In addition, the attractive interaction induces a small bandgap that deteriorates the thermal and optical properties of the system. In contrast, in the presence of a repulsive interaction between the B and N atoms, the AA-stacking is converted to a AB-stacking with a more stable structure. Improved mechanical properties such as higher Young modulus, the ultimate strength and stress, fracture strength are obtained comparing to the AA-stacked BN-codoped BLG. Furthermore, a larger bandgap of the AB-stacked bilayer enhances the thermal and the optical characteristics of the system.

Keywords: Thermoelectric, Bilayer graphene, DFT, Electronic structure, Optical properties, and Stress-strain curve

1. Introduction

Graphene has been considered as a promising material for applications in the fields of sensors, photonics, and electronic devices because of its excellent characteristics such as optical transparency, low density, high carrier mobility, and chemical stability [1, 2, 3, 4]. Combining two layers of graphene in a specific configuration called bilayer graphene is also a high-potential material with possible applications in electronics and optics [5, 6, 7, 8]. It has been experimentally shown that BLG has a number of remarkable characteristics such as outstanding electrical, mechanical and chemical performance leading to a great flexible transparent electrodes used in touch-screen devices [9], high-switching ratio digital transistors [10], and efficient infrared detectors [11]. Stiffness and flexibility properties of BLG make it a great candidate for fuel cells and a material for use in structural composite applications [12].

The aforementioned properties of BLG can be improved by tuning the interaction between the graphene layers, or the van der Waals interactions appearing between the layers [13, 14]. The DFT-D technique, dispersion-corrected density functional theory, has been used to describe the

interlayer interaction energy of BLG with high accuracy [15]. It has been found that the interlayer electron motion is affected by the atomic orientation of the two layers [16, 17]. The atomic orientation controls the strength of the interlayer van der Waals bonding. The interlayer electron interaction is influenced by the stacking configuration of the BLG leading to interesting physical properties. For instance, a moiré pattern has been observed due to the interaction between the layers for twisted BLG [18] with extraordinary optical properties found [19, 20, 21]. Furthermore, a relatively weak strength of interlayer interaction, and low energetic cost of relative translation of the layers, has been seen for AA-stacking BLG [22]. Compared with other stacking structures, AA- and twisted-stacking, very strong coupling exists between the two layers of AB-stacked BLG, which has the lowest energy and the most stable structure among the different orientations [23]. Strong coupling between the layers improves and leads to numerous physically interesting properties in BLG. In recent experimental work, the stacking orientation of BLG is investigated and it is found that the orientation of BLG could be changed from weak stacking coupling to AB strong stacking coupling. In addition, a reduction in the interlayer distance is considered in a high-pressure environment to detect orientation changes [24]. We therefore, believe that the stacking configuration of BLG is still

Email address: nzar.r.abdullah@gmail.com (Nzar Rauf Abdullah)

challenging and further work is needed to clearly the situation.

In the present paper, we try to control the distance and interlayer interactions of AA-stacked BLG by boron (B) and Nitrogen (N) dopant atoms. We will show how the AA-stacking with a weak interlayer interaction can be converted into a AB-stacking with a strong interlayer interaction by doping of B and N atoms in the BLG. More precisely, the conversion of AA- to AB-stacked BLG will be achieved by controlling the dimer positions of the B and N atoms in the hexagonal structure of the graphene [25]. In addition, the electronic, mechanical, thermal, and optical properties of the system will be shown for both AA- and AB-stacked BLG, and one can see significant improvement of the physical properties of the AB-stacked BLG in our study [26, 27].

In Sec. 2 the BLG structure is briefly over-viewed. In Sec. 3 the main achieved results are analyzed. In Sec. 4 the conclusion of the results is presented.

2. Computational technique

We assume a pure BLG and BN-doped BLG with different B and N atom configurations. The density functional theory (DFT) techniques based on the local density approximation (LDA) implemented in Quantum espresso package have been used to study physical properties of our models [28, 29]. A periodic boundary conditions are applied to a $5.65 \text{ \AA} \times 2.44 \text{ \AA} \times 20 \text{ \AA}$ model cell of pure BLG. The Brillouin zone is sampled with k -point grids from $10 \times 10 \times 1$ to $20 \times 20 \times 1$, and the basis set is plane waves with a maximum kinetic energy of 680-1360 eV [30]. The spacing of the real space grid used to calculate the Hartree, the exchange and the correlation contribution of the total energy 1360 eV. The van der Waals interaction is included in the exchange (XC) functional, and the structures are relaxed until the forces on each atom were less than 0.001 eV/\AA .

The XCrySDen is used to visualize all the structures [31, 32]. In addition, the Boltzmann transport properties software package (BoltzTraP) is employed to study the thermal properties of the systems [33]. The BoltzTraP code uses a mesh of band energies and has an interface to the QE package. The optical characteristics of the systems are obtained by the QE code. Optical calculations are performed using a $100 \times 100 \times 2$ optical mesh and an optical broadening of 0.1 eV .

3. Results

Pristine BLG and BN-codoped BLG are shown in Fig. 1, with the B (red) atom fixed at a para-position in the top layer, and the N (blue) atom is doped in the bottom layer at a para-position corresponding to the B atom (BLG-1), the meta-position (BLG-2), the ortho-position (BLG-3), and a para-position at a site opposite to the B atom (BLG-4). The position of the B and N atoms together forms

different isomers which are called a para-isomer for BLG-1, a meta-isomer for BLG-2, an ortho-isomer for BLG-3, and a para-isomer for BLG-4.

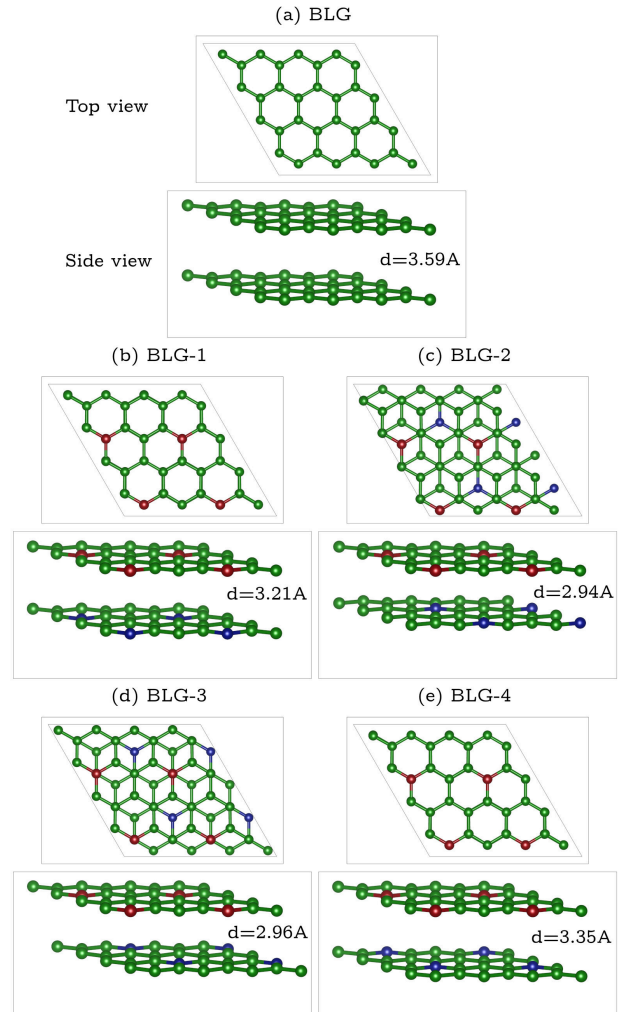


Figure 1: Pristine BLG (a) and BN-codoped BLG (b-d) where the C, B, and N atoms are green, red, and blue colored, respectively, the B(N) atom is doped in top(bottom) layer. The B atoms is fixed at a para-position in the top layers of all structures, but the N atom is doped in a para-position at a site corresponding to the B atom in BLG-1, a meta-position in BLG-2, ortho-position in BLG-3, and para-position at a site opposite to the B atom in BLG-4 in the bottom layer. d indicates the interlayer distances.

The structural parameters calculated for BLG and BN-codoped BLG are presented in Tab. 1. The calculation of the structural parameters indicate that in the presence of the B and N atoms the average bond lengths of C-C, C-B, and C-N are slightly changed for all BN-codoped BLGs. This is due to the larger and the smaller atomic radius of the B and the N atoms, respectively, compared to the atomic radii of a C atom [34]. Furthermore, the average lattice parameters of the BN-codoped structures are increased compared to the pure BLG indicating a super-cell expansion of the BN-codoped BLG. It is found that the C-C bond length, the lattice parameters, and the inter-

Table 1: The average bond lengths of C-C, C-B, and C-N, lattice parameters, a , interlayer distance, d , interlayer interaction energy, E_{in} , and distance between B and N atoms, d_{BN} , for BLG and BN-codoped BLG structures. The unit of all parameters except ΔE is Å.

Structure	C-C	C-B	C-N	a	d	ΔE (eV)	d_{BN}
BLG	1.42	—	—	2.44	3.59	—	—
BLG-1	1.413	1.46	1.417	2.468	3.21	-3.25	3.21
BLG-2	1.418	1.458	1.419	2.471	2.94	2.45	4.11
BLG-3	1.415	1.458	1.419	2.471	2.96	2.39	4.1
BLG-4	1.416	1.458	1.418	2.465	3.35	-4.35	4.4

layer spacing of our pure BLG are consistent with previous studies [35, 36]. The C-B and C-N bond lengths and lattice parameters of BN-codoped BLG agree very well with Alattas and Schwingschlögl [37].

3.1. Interlayer Interaction

The key point of this work is the interlayer interaction due to the B and N doped atoms. There are several details that should be considered to analyse the components or the sources of the interlayer interactions in BLG. We take into account the van der Waals interactions which introduce a non-bonding potential between the layers of BLG. The Van der Waals interaction is a dipole-dipole interaction that can dominate other interactions if the distance between dipoles is around and beyond 4-5 Å [38, 39, 40]. This type of interaction does not play a key role in our systems as the distance between the layer does not reach that limit (see Tab. 1). Other types of interactions dominate over the weak dipole-dipole interaction in our system. More important is the interaction that arises due to the sp^3 bonding between the two layers of the BLG. This type of interaction is best studied by incrementally moving two atoms with the same planar coordinates (one in the upper layer and the other one in the lower layer) to the sp^3 bond distance which is about 1.54 Å and allow the structure to relax [41]. Again, we do not expect this type of interaction to be important as our models have larger interlayer distance. The third type of interaction is a nonbonding interaction between the layers of a BLG that could be either a repulsive or attractive [42]. This type of interaction is effective if the interlayer distance is around 2-4 Å. We assume this type of interaction to play an important role between the layers, and the interaction energy between two dopant atoms in a structure is given by [43]

$$\Delta E = E_2 - E_0 + 2 \times E_1 \quad (1)$$

where E_0 , E_1 and E_2 are the total energies of the systems with zero, one, and two dopant atoms, respectively. The obtained interaction energies of all BN-codoped systems are presented in Tab. 1. It has been shown that the interaction energy in BN-codoped graphene varies inversely with the distance between the B and N atoms because of the nature of the Coulombic electrostatic interaction, and the interaction strength is almost zero when the separation distance is greater than or equal to 4.0 Å [43]. The

value of ΔE can have a negative or a positive sign indicating that the interaction between the B and N atoms is attractive or repulsive, respectively.

At first the sight, one can see the interaction between the B and the N atoms leading to an attractive between the layers of BLG-1, as the interaction energy is negative when both the B and N atoms sit on the same isomer position, para-position, but in different layers. Consequently, the 'Coulomb electrostatic potential' between the B and N atoms is directly along the π -bond directions on the same line perpendicular to both the B and N atoms. The Coulomb electrostatic force only affects the interlayer spacing in the z -direction and does not influence the atomic positions of both layers in the xy -plane. In this case, the AA-stacking behavior of BLG-1 is unchanged. The same scenario can be applied to BLG-4 when the B and N atoms sit in opposite para-positions. The separation between the B and N atom is large here, 4.4 Å, leading to a weak interaction energy and interlayer interaction. So, the interaction between the B and N atom does not influence the structural property of the system and the AA-stacking of BLG-4 is again unchanged. Notice that the interlayer distance of BLG-4 is maximum among all BN-codoped structures and it is also close to the interlayer distance of pure BLG confirming a weak interaction between the dopant atoms.

The most interesting point here is the interlayer interaction in BLG-2 and BLG-3 due to the relative position of the B and N atoms that does not only decrease the interlayer distance, but also converts the AA-stacked BLG to an AB-stacked one (see Fig. 1c-d). This is the key point of our study. In these two structures, the B and N atoms are doped in such a way that a meta-isomer in BLG-2, and an ortho-isomer in BLG-3 are formed as we mentioned before. In these two isomers, the 'tangential Coulomb electrostatic force' present between the B and N atoms generates a repulsive force between the B and N atoms. Consequently, a diffusion and depletion between the layers emerges activating a conversion from the AA-stacking to an AB-stacked structure. Our results for the interaction energy shown in Tab. 1 confirms the repulsive force between the B and N atoms in these two structures as their interaction energies are positive. The diffusion process between the layers continues until the distance between the B and N atoms approaches 4.0 Å, which is the equilibrium imposed by

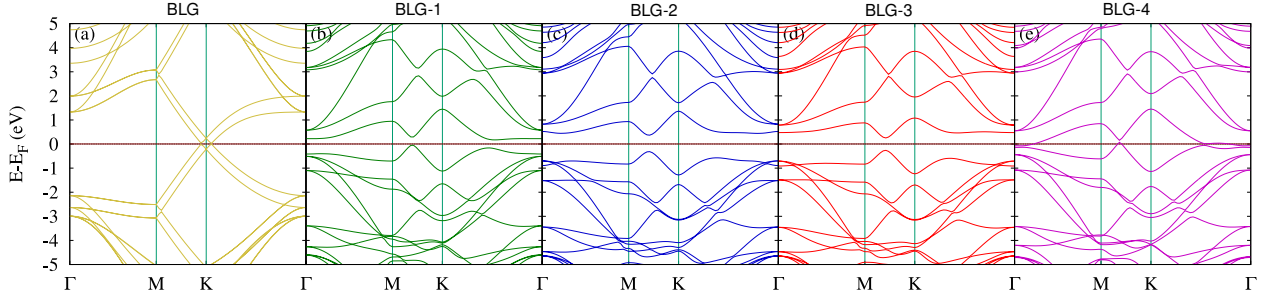


Figure 2: Dispersion energy or electronic band structure of pure BLG (a), and BN-codoped BLG (b-e) are shown. The Fermi energy is set to zero.

the effective interaction of the two dopant atoms forming an effective interaction [43]. The distance between the B and N atoms after full relaxation in BLG-2 (BLG-3) is 4.11 (4.1 Å), respectively. Any change of physical properties including the layer conversion arising from the isomer position of the dopant atoms is called the effect of isomerization [44, 45].

3.2. Band structure and DOS

In order to understand the physical properties of BN-codoped BLG, such as thermal and optical characteristics, we need to present the dispersion energy of the structures. In Fig. 2, the dispersion energy or the electronic band structures of pure BLG (a), and BN-codoped BLG (b-e) are displayed. In Fig. 2(a) the dispersion of pure BLG has multiple linear dispersion bands forming π_1 , π_2 and π_1^* , π_2^* that touch at the K-point of the first Brillouin zone. So, the intersection of the conduction and valence bands is located symmetrically near the K-point. The linear dispersion bands are mainly due to the electronic interlayer coupling that is suppressed by the Pauli repulsion between the graphene layers [46]. The linear dispersion of the AA-stacked BLG has been experimentally confirmed [47].

The computed electronic band structures of BLG-1, BLG-2, and BLG-3, based on LDA calculation, show a semiconducting property with an indirect bandgap of BLG-1, and a direct bandgap of the BLG-2 and BLG-3 structures. The band structure of BLG-4 exhibits a metallic behavior as the lowest conduction band crosses the Fermi energy near the Γ -point. The origin of bandgap opening comes from the redistribution of surface charge due to the B and N atoms that breaks the local symmetry of the BLG. The redistribution of the charge density of the BN-codoped BLG gives rise to the separation of the valence band and conduction band at the Dirac point. The B atoms lead to band shift below the Fermi level, and the N atoms above the Fermi level, such that the counterbalance of both creates a gap at the Fermi level. Furthermore, the electrostatic Coulomb dipole interaction between the B and N atoms is also important in breaking the symmetry of BLG and thus to the band gap opening [44]. A narrowing of the bandgap in BLG is also induced by interlayer

interaction [48]. The computed bandgaps of the BLG-1, BLG-2, and BLG-3 are 0.346, 0.685, and 0.515 eV, respectively. It is interesting to see that the bandgaps of the BLG-2 and BLG-3 with the repulsive interaction between the B and N atoms are relatively larger than those of the BLG-1 and BLG-4 with the attractive interaction between the B and N atoms. It has been confirmed that the repulsive interaction between the layers forms a direct and large bandgap, while an attractive interaction induces an indirect and small bandgap in both the AA- and the AB-stacked BLG with B and N dopant atoms [49]. Our results for the band dispersion and the bandgaps agree very well with recent results for BN-codoped BLG in which the BLG is doped with one B atom in one layer and one N atom in the other [37].

The computed partial density of states (PDOS) of pure BLG and BN-codoped BLG are presented in Fig. 3. It is clearly seen that the maximum of the valence band and the minimum of the conduction band for pure-BLG are totally formed by the four p_z π -bands around the Fermi energy. Furthermore, the s and $p_{x,y}$ contribute to the lower part of the valence band and upper part of the conduction band as is expected for pure BLG [50, 51].

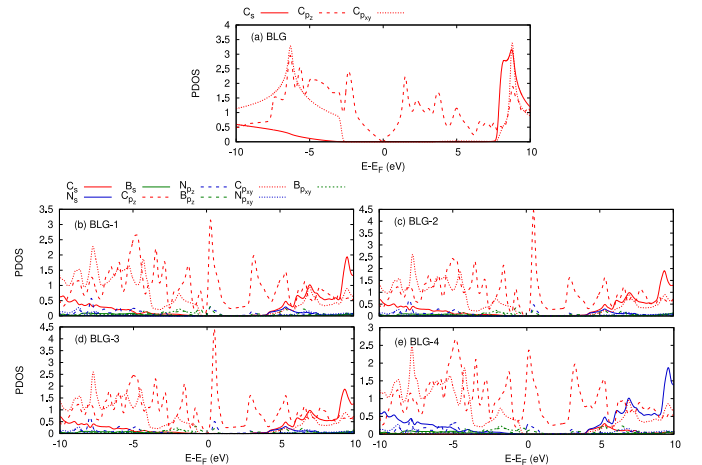


Figure 3: Partial density of states (PDOS) of pure BLG (a), and BN-codoped BLG (b-e) are shown. The Fermi energy is set to zero.

The PDOS of the BN-codoped BLG is analyzed showing that in all four cases of a BN-codoped BLG the higher

	Zigzag				Armchair			
	YM (TPa)	UTS	F-strength	F-strain (%)	YM (TPa)	UTS	F-strength	F-strain (%)
BLG	0.99	99.47	99.47	15.12	0.99	96.06	96.06	12.66
BLG-1	0.65	58.55	58.55	12.14	0.65	56.73	56.73	11.24
BLG-2	0.856	74.89	70.58	12.45	0.858	77.66	61.73	18.07
BLG-3	0.855	77.82	77.82	12.14	0.875	78.04	71.58	13.76
BLG-4	0.608	55.67	55.67	12.14	0.622	59.92	59.92	11.24

Table 2: The Young modulus (YM), the ultimate strength (UTS), the fracture strength (F-strength), and the fracture strain (F-strain) for BLG and BN-codoped BLG structures in the zigzag and armchair directions. The unit of UTS and F-stress is GPa.

valence bands have a contribution from the p_z of the C and B atoms, and the lower conduction bands are formed by the p_z of the C, B and N atoms. We note that the major contribution to the π -bands comes from the C atoms. More precisely, the contribution of the B and N atoms around the Fermi energy is slightly higher for the BLG-2 and BLG-3, where the a repulsive interaction between the B and N atoms exists. It is also expected that the contribution of both the s and $p_{x,y}$ by the B and N atoms are increased at the lower valence and the upper conduction bands.

3.3. Mechanical properties

The DFT calculations can be used to investigate the stress-strain curves of our systems. We apply uniaxial tensile simulations to probe the stress-strain properties. The load is gradually applied to a specific direction of the structure, the zigzag or armchair directions [52]. During a uniaxial tensile loading, the periodic dimension along the loading direction is increased step-by-step with a fixed strain of 0.02.

The stress-strain curves of pristine BLG as well as the ones for the BN-codoped BLG are presented in Fig. 4 for zigzag (a), and armchair (b) directions. The strain-stress curves depend on stability of the structures in which the most stable structure has the highest stress-strain curve. One can see that the stress-strain curves of BN-codoped BLG are lower than those for the pure BLG for both directions over the entire values of the strain. This is due to the more stable C-C bond than the B-C or N-C bond. The bond energy of C-C is 3.71 eV which is greater than that of C-N (2.83 eV) and C-B (2.59 eV) [53, 54]. Consequently, the structure with a higher number of C-C bonds will be more stable than the others. This is the reason for higher stress-strain curves of pure the BLG compared to the BN-codoped BLG.

In addition, a structure with the lowest total energy will be the most stable structure [46]. Our DFT calculations of the total energy confirm that the most stable structures among the BN-codoped BLG are BLG-2 and BLG-3. These two structures have lower total energies

than BLG-1 and BLG-4. Therefore, the BLG-2 and BLG-3 structures with repulsive interaction between the B and N atoms have higher stress-strain curves than the BLG-1 and BLG-4 structures with an attractive interaction. This also refers to AB-stacked BLG-2 and BLG-3 formed by the repulsive interaction in which the AB-stacked shapes have more energetically stable structure than AA-stacked one.

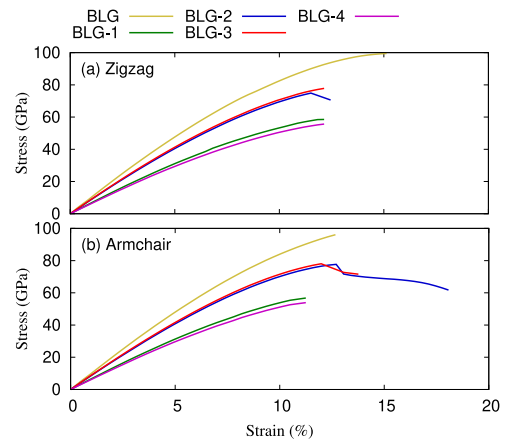


Figure 4: Stress-strain curves for pure BLG (golden), BLG-1 (green), BLG-2 (blue), BLG-3 (red), and BLG-4 (purple) in the zigzag (a) and armchair (b) directions.

The values of the ultimate strength (UTS), the Young modulus (YM), the fracture strength (F-strength), and the fracture strain (F-strain) can be computed and their values for all structures are presented in Tab. 2. It is known that the YM defines the tensile stiffness of a structure. In a small range of strain of about a few percent (strain < 4%), when the tensile strain increases, the stress that the system experienced enlarges linearly for the BLG and BN-codoped BLG structures. From the linear regime of the curves, one can calculate the Young's moduli, which are basically the initial slope of the stress-strain curves. The strain-stress curve of pure BLG reveals the YM to be 0.99 TPa for both the zigzag and armchair directions in good agreement with the theoretical value of 0.96 TPa [55], and the experimental value of 1.0 TPa [56].

When a large strain is applied, the stress response of a system is non-linearly up to the strain for which the system

fails. The UTS defines the maximum stress that a structure can withstand while being stretched. The UTS for pure BLG in the zigzag direction is slightly higher than that of the armchair one. Furthermore, the F-strength, also known as breaking strength, is the stress at which a structure fails via fracture, while F-strain reflects flexibility of the system. The values of the F-strength and the F-strain in the zigzag direction of the pure BLG is higher than that of the armchair direction which can be related to the anisotropy of the system.

It is interesting to see that the YM, UTS, F-strength, and F-strain of the BLG-1 and BLG-4 are all decreased compared to the pure BLG. These two structures have the AA-stacking shape and they are less stable leading to smaller values of the YM, UTS, F-strength, and F-strain. In contrast, the BLG-2 and BLG-3 with the AB-stacking shape are more stable leading to higher YM, UTS, F-strength, and F-strain compared to the BLG-1 and BLG-4 structures. We should remember that all the BN-codoped BLG structures have the same number of C-B and C-N bonds, we therefore emphasize that the number of C-B and C-N bonds does not play a role when we compare the stress-strain curves of these four structures.

3.4. Thermal properties

The thermal characteristics of our structures at the low temperature ranging from 20 to 160 K are considered where the phonons are inactive [57, 32].

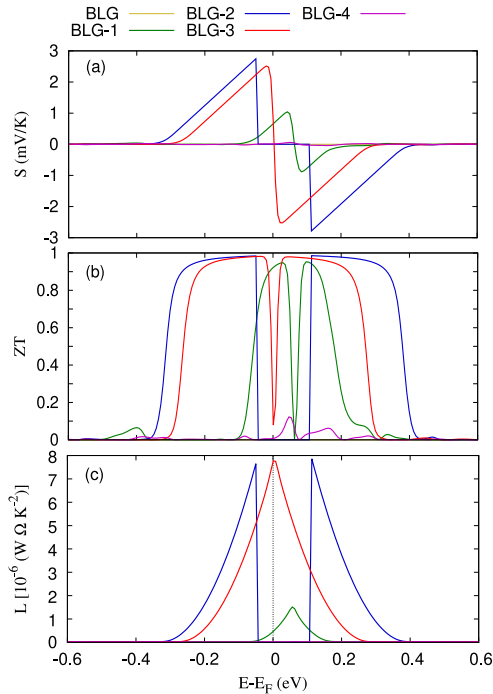


Figure 5: Seebeck coefficient (a), figure of merit (ZT), and Lorentz number (L) versus energy for pure BLG (golden), BLG-1 (green), BLG-2 (blue), BLG-3 (red), and BLG-4 (purple). The Fermi energy is set to zero.

In such a low temperature range, the electrons deliver

the main contribution to the thermal properties. Figure 5 presents the Seebeck coefficient, S , (a), the figure of merit, ZT , (b), and Lorentz number, L , (c) as a function of energy for pure BLG and BN-codoped BLG structures. A good thermoelectric material should have a low thermal conductivity, and a high S and electrical conductivity. The thermoelectric performance of a monolayer and a BLG is poor because of closed bandgaps, leading to a small S [58, 59]. This is also seen for pure BLG shown in Fig. 5(a), where the S has an extremely small value which is almost invisible in the figure. Similarly, this gives rise to very small value of ZT and L for pure BLG as well.

Asymmetric peaks in the PDOS close to the highest occupied state shown in Fig. 3, and the opening up of a bandgap are expected to increase the S , ZT and L in BLG-1, BLG-2 and BLG-3 structures [60, 61]. A small bandgap of BLG-1 induces small S , ZT and L , while the largest bandgap of BLG-2 gives the maximum values of S , ZT and L . Therefore, one can expect a higher thermoelectric performance for the BLG-2.

3.5. Optical responses

We explore the optical properties of pure BLG and BN-codoped BLG which may be interesting for optoelectronic use of graphene-based materials. The rise in interest of BLG in optoelectronics is presented by its applications ranging from solar cells and light-emitting devices to touch screens, photo-detectors and ultrafast lasers. These all come from the unique optical and electronic properties of BLG and their relevance for nano-photonics [62, 27, 63, 64].

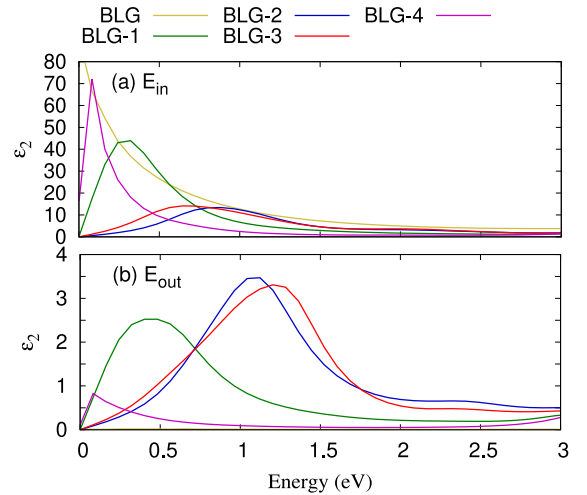


Figure 6: Imaginary part of dielectric function, ϵ_2 , versus energy for pure BLG (golden), BLG-1 (green), BLG-2 (blue), BLG-3 (red), and BLG-4 (purple), in the E_{in} (a), and E_{out} (b).

In our pure BLG, two main peaks in the imaginary part of the dielectric function are formed at 4.01 and 14.03 eV representing π to π^* transitions when the applied electric field is parallel to the BLG structure, and two peaks at 11.4 and 14.42 eV corresponding to the σ and σ^* transition are

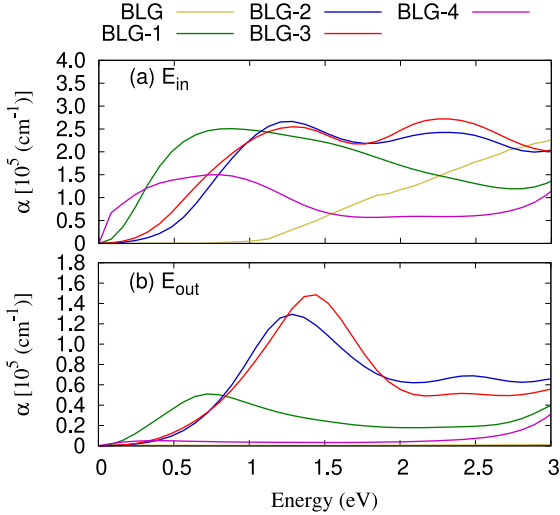


Figure 7: Absorption coefficient versus energy for pure BLG (golden), BLG-1 (green), BLG-2 (blue), BLG-3 (red), and BLG-4 (purple), in the E_{in} (a), and E_{out} (b).

seen for perpendicular applied electric field (not shown). We observe a red shift in all four peaks in the presence of BN-codoped BLG with more or less the same intensity of the peaks (not shown). The red shift of the peaks is caused by the decreased energy spacing between the π and the π^* , and the σ and the σ^* along the Γ -M and the M-K directions (see Fig. 2). The details of these transitions are shown in our recent publication [49]. In addition to these peaks, extra peaks in the low energy range from 0 to 3.0 eV, towards the visible range of radiation, are found corresponding to the bandgap opening of the structures.

In this work we focus on the peaks formed at the low energies. In Fig. 5 and Fig. 6 the imaginary part of dielectric function and the absorption coefficient are shown, respectively, for a parallel or in-plane, E_{in} , (a) and a perpendicular or out of plane, E_{out} , (b) electric field applied to the BLG structure [65, 66, 67]. The peaks in the imaginary part of the dielectric function in the presence of E_{in} are due to optical transitions in the bandgap or very close to the bandgap. We therefore see peaks formed at different values of energy indicating the bandgap energy. We should remember that values of the bandgaps are underestimate as the DFT with a local density approximation has been used here. Therefore, the peak position is not exactly equal to the bandgap energy. Furthermore, the peaks in the presence of E_{out} represent the σ and σ^* transitions around the Γ -points. It can clearly be seen that the peak intensity of ϵ_2 in the presence of E_{out} for BLG-2 and BLG-3 are maximum while a minimum peak intensity is found for BLG-4.

In addition, the energy loss-function, EELS characterizing inelastic scattering processes of the BN-codoped BLG structures is calculated for light polarization E_{in} and E_{out} , and compared to BLG. The EELS is displayed in Fig. 8 for E_{in} (a), and E_{out} (b) in a low energy range.

We observe from the plots of EELS that with increas-

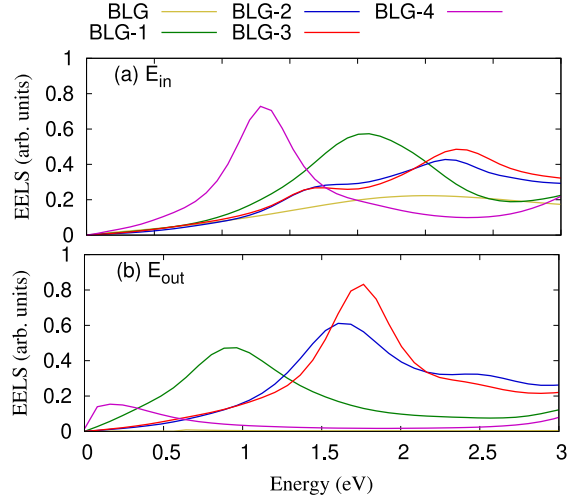


Figure 8: Energy loss-function, EELS, versus light energy for pure BLG (golden), BLG-1 (green), BLG-2 (blue), BLG-3 (red), and BLG-4 (purple), in the E_{in} (a), and E_{out} (b).

ing the bandgap of the BN-codoped structures the peak is shifted to higher energy indicating that an inelastic scattering process occurs at a high energy of the light for the structure with a larger bandgap.

4. Conclusion

This study uses DFT techniques based on the local density (LDA) approach to investigate electronic, mechanical, thermal and optical properties of BLG systems with Boron and Nitrogen dopant atoms. The DFT is implemented in Quantum espresso code and the Boltztrap package is used for further properties of the system. We show that the bandgap of AA-stacked BN-codoped BLG decreases with increasing interlayer spacing, while the bandgap of AB-stacked BN-codoped BLG increases. In addition, the attractive interaction between the B and the N atoms deteriorates the mechanical, thermal and optical properties of the system. In contrast, a repulsive interaction improve the high mechanical, thermal and optical characteristics of the system. Our results are relevant for optoelectronic applications of graphene-based devices.

5. Acknowledgment

This work was financially supported by the University of Sulaimani and the Research center of Komar University of Science and Technology. The computations were performed on resources provided by the Division of Computational Nanoscience at the University of Sulaimani.

References

- [1] D. Kwong Hong Tsang, T. J. Lieberthal, C. Watts, I. E. Dunlop, S. Ramadan, A. E. del Rio Hernandez, N. Klein, [Chemically functionalised graphene fet biosensor for the label-free sensing](#)

- of exosomes, *Scientific Reports* 9 (1) (2019) 13946. doi:10.1038/s41598-019-50412-9.
URL <https://doi.org/10.1038/s41598-019-50412-9>
- [2] K. Chen, X. Zhou, X. Cheng, R. Qiao, Y. Cheng, C. Liu, Y. Xie, W. Yu, F. Yao, Z. Sun, F. Wang, K. Liu, Z. Liu, Graphene photonic crystal fibre with strong and tunable light-matter interaction, *Nature Photonics* 13 (11) (2019) 754–759. doi:10.1038/s41566-019-0492-5.
URL <https://doi.org/10.1038/s41566-019-0492-5>
- [3] E. McCann, M. Koshino, The electronic properties of bilayer graphene, *Reports on Progress in Physics* 76 (5) (2013) 056503. doi:10.1088/0034-4885/76/5/056503.
URL <https://doi.org/10.1088/2F0034-4885/2F76%2F5%2F056503>
- [4] V. Gudmundsson, H. Gestsson, N. R. Abdullah, C.-S. Tang, A. Manolescu, V. Moldoveanu, Coexisting spin and rabi oscillations at intermediate time regimes in electron transport through a photon cavity, *Beilstein Journal of Nanotechnology* 10 (1) (2019) 606–616.
- [5] J. Nilsson, A. H. Castro Neto, F. Guinea, N. M. R. Peres, Electronic properties of bilayer and multilayer graphene, *Phys. Rev. B* 78 (2008) 045405. doi:10.1103/PhysRevB.78.045405.
URL <https://link.aps.org/doi/10.1103/PhysRevB.78.045405>
- [6] D. S. L. Abergel, V. I. Fal'ko, Optical and magneto-optical far-infrared properties of bilayer graphene, *Phys. Rev. B* 75 (2007) 155430. doi:10.1103/PhysRevB.75.155430.
URL <https://link.aps.org/doi/10.1103/PhysRevB.75.155430>
- [7] C.-S. Tang, J.-A. Keng, N. R. Abdullah, V. Gudmundsson, Spin magneto-transport in a rashba-dresselhaus quantum channel with single and double finger gates, *Physics Letters A* 381 (17) (2017) 1529 – 1533. doi:https://doi.org/10.1016/j.physleta.2017.03.005.
URL <http://www.sciencedirect.com/science/article/pii/S0375960117302293>
- [8] N. R. Abdullah, C.-S. Tang, A. Manolescu, V. Gudmundsson, Oscillations in electron transport caused by multiple resonances in a quantum dot-qed system in the steady-state regime, *Physica E: Low-dimensional Systems and Nanostructures* 123 (2020) 114221. doi:https://doi.org/10.1016/j.physe.2020.114221.
URL <http://www.sciencedirect.com/science/article/pii/S1386947719311750>
- [9] S. Bae, H. Kim, Y. Lee, X. Xu, J.-S. Park, Y. Zheng, J. Balakrishnan, T. Lei, H. Ri Kim, Y. I. Song, Y.-J. Kim, K. S. Kim, B. Özyilmaz, J.-H. Ahn, B. H. Hong, S. Iijima, Roll-to-roll production of 30-inch graphene films for transparent electrodes, *Nature Nanotechnology* 5 (8) (2010) 574–578. doi:10.1038/nnano.2010.132.
URL <https://doi.org/10.1038/nnano.2010.132>
- [10] K. Yan, H. Peng, Y. Zhou, H. Li, Z. Liu, Formation of bilayer bernal graphene: Layer-by-layer epitaxy via chemical vapor deposition, *Nano Letters* 11 (3) (2011) 1106–1110, pMID: 21322597. arXiv:https://doi.org/10.1021/nl104000b, doi:10.1021/nl104000b.
URL <https://doi.org/10.1021/nl104000b>
- [11] Y. Zhang, T.-T. Tang, C. Girit, Z. Hao, M. C. Martin, A. Zettl, M. F. Crommie, Y. R. Shen, F. Wang, Direct observation of a widely tunable bandgap in bilayer graphene, *Nature* 459 (7248) (2009) 820–823. doi:10.1038/nature08105.
URL <https://doi.org/10.1038/nature08105>
- [12] D. A. Dikin, S. Stankovich, E. J. Zimney, R. D. Piner, G. H. B. Dommett, G. Evmenenko, S. T. Nguyen, R. S. Ruoff, Preparation and characterization of graphene oxide paper, *Nature* 448 (7152) (2007) 457–460. doi:10.1038/nature06016.
URL <https://doi.org/10.1038/nature06016>
- [13] Y. J. Dappe, M. A. Basanta, F. Flores, J. Ortega, Weak chemical interaction and van der waals forces between graphene layers: A combined density functional and intermolecular perturbation theory approach, *Phys. Rev. B* 74 (2006) 205434. doi:10.1103/PhysRevB.74.205434.
URL <https://link.aps.org/doi/10.1103/PhysRevB.74.205434>
- [14] K. Tanaka, H. Aoki, H. Ago, T. Yamabe, K. Okahara, Interlayer interaction of two graphene sheets as a model of double-layer carbon nanotubes, *Carbon* 35 (1) (1997) 121 – 125. doi:https://doi.org/10.1016/S0008-6223(96)00124-8.
URL <http://www.sciencedirect.com/science/article/pii/S0008622396001248>
- [15] I. V. Lebedeva, A. A. Knizhnik, A. M. Popov, Y. E. Lozovik, B. V. Potapkin, Interlayer interaction and relative vibrations of bilayer graphene, *Phys. Chem. Chem. Phys.* 13 (2011) 5687–5695. doi:10.1039/C0CP02614J.
URL <http://dx.doi.org/10.1039/C0CP02614J>
- [16] J. S. Alden, A. W. Tsen, P. Y. Huang, R. Hovden, L. Brown, J. Park, D. A. Muller, P. L. McEuen, Strain solitons and topological defects in bilayer graphene, *Proceedings of the National Academy of Sciences* 110 (28) (2013) 11256–11260. arXiv:https://www.pnas.org/content/110/28/11256.full.pdf, doi:10.1073/pnas.1309394110.
URL <https://www.pnas.org/content/110/28/11256>
- [17] W. Yan, W.-Y. He, Z.-D. Chu, M. Liu, L. Meng, R.-F. Dou, Y. Zhang, Z. Liu, J.-C. Nie, L. He, Strain and curvature induced evolution of electronic band structures in twisted graphene bilayer, *Nature Communications* 4 (1) (2013) 2159. doi:10.1038/ncomms3159.
URL <https://doi.org/10.1038/ncomms3159>
- [18] L. Huder, A. Artaud, T. Le Quang, G. T. de Laissardière, A. G. M. Jansen, G. Lapertot, C. Chapelier, V. T. Renard, Electronic spectrum of twisted graphene layers under heterostrain, *Phys. Rev. Lett.* 120 (2018) 156405. doi:10.1103/PhysRevLett.120.156405.
URL <https://link.aps.org/doi/10.1103/PhysRevLett.120.156405>
- [19] Q. Ye, J. Wang, Z. Liu, Z.-C. Deng, X.-T. Kong, F. Xing, X.-D. Chen, W.-Y. Zhou, C.-P. Zhang, J.-G. Tian, Polarization-dependent optical absorption of graphene under total internal reflection, *Applied Physics Letters* 102 (2) (2013) 021912. arXiv:https://doi.org/10.1063/1.4776694, doi:10.1063/1.4776694.
URL <https://doi.org/10.1063/1.4776694>
- [20] N. R. Abdullah, Rabi-resonant and intraband transitions in a multilevel quantum dot system controlled by the cavity-photon reservoir and the electron-photon coupling, *Results in Physics* 15 (2019) 102686. doi:10.1016/j.rinp.2019.102686.
URL <http://www.sciencedirect.com/science/article/pii/S221137971932251X>
- [21] M. De Corato, C. Cocchi, D. Prezzi, M. J. Caldas, E. Molinari, A. Ruini, Optical properties of bilayer graphene nanoflakes, *The Journal of Physical Chemistry C* 118 (40) (2014) 23219–23225. arXiv:https://doi.org/10.1021/jp504222m, doi:10.1021/jp504222m.
URL <https://doi.org/10.1021/jp504222m>
- [22] A. Vuong, T. Trevethan, C. D. Latham, C. P. Ewels, D. Erbahar, P. R. Briddon, M. J. Rayson, M. I. Heggie, Interlayer vacancy defects in AA-stacked bilayer graphene: density functional theory predictions, *Journal of Physics: Condensed Matter* 29 (15) (2017) 155304. doi:10.1088/1361-648x/aa5f93.
URL <https://doi.org/10.1088/2F1361-648x/2Faa5f93>
- [23] X. Chen, F. Tian, C. Persson, W. Duan, N.-x. Chen, Interlayer interactions in graphites, *Scientific Reports* 3 (1) (2013) 3046. doi:10.1038/srep03046.
URL <https://doi.org/10.1038/srep03046>
- [24] Z. Chen, Y. Sui, J. Li, H. Kang, S. Wang, S. Zhao, X. Gao, S. Peng, Z. Jin, X. Liu, Y. Zhang, G. Yu, Conversion of the stacking orientation of bilayer graphene through high-pressure treatment, *Carbon* 172 (2021) 480 – 487. doi:https://doi.org/10.1016/j.carbon.2020.10.026.
URL <http://www.sciencedirect.com/science/article/pii/S0008622320309908>
- [25] N. R. Abdullah, D. A. Abdalla, T. Y. Ahmed, S. W. Abdulqadr, H. O. Rashid, Effect of bn dimers on the stability, electronic, and

- thermal properties of monolayer graphene, *Results in Physics* 18 (2020) 103282. doi:<https://doi.org/10.1016/j.rinp.2020.103282>.
URL <http://www.sciencedirect.com/science/article/pii/S2211379720317496>
- [26] N. R. Abdullah, C.-S. Tang, A. Manolescu, V. Gudmundsson, The photocurrent generated by photon replica states of an off-resonantly coupled dot-cavity system, *Scientific Reports* 9 (1) (2019) 14703. doi:[10.1038/s41598-019-51320-8](https://doi.org/10.1038/s41598-019-51320-8).
URL <https://doi.org/10.1038/s41598-019-51320-8>
- [27] N. R. Abdullah, C.-S. Tang, A. Manolescu, V. Gudmundsson, Manifestation of the purcell effect in current transport through a dot-cavity-qed system, *Nanomaterials* 9 (7) (2019) 1023. doi:[10.3390/nano9071023](https://doi.org/10.3390/nano9071023).
URL <http://dx.doi.org/10.3390/nano9071023>
- [28] P. Giannozzi, S. Baroni, N. Bonini, M. Calandra, R. Car, C. Cavazzoni, D. Ceresoli, G. L. Chiarotti, M. Cococcioni, I. Dabo, A. D. Corso, S. de Gironcoli, S. Fabris, G. Fratesi, R. Gebauer, U. Gerstmann, C. Gougoussis, A. Kokalj, M. Lazzeri, L. Martin-Samos, N. Marzari, F. Mauri, R. Mazzarello, S. Paolini, A. Pasquarello, L. Paulatto, C. Sbraccia, S. Scandolo, G. Sclauzero, A. P. Seitsonen, A. Smogunov, P. Umari, R. M. Wentzcovitch, QUANTUM ESPRESSO: a modular and open-source software project for quantum simulations of materials, *Journal of Physics: Condensed Matter* 21 (39) (2009) 395502. doi:[10.1088/0953-8984/21/39/395502](https://doi.org/10.1088/0953-8984/21/39/395502).
URL <https://doi.org/10.1088/0953-8984/21/39/395502>
- [29] P. Giannozzi, O. Andreussi, T. Brumme, O. Bunau, M. B. Nardelli, M. Calandra, R. Car, C. Cavazzoni, D. Ceresoli, M. Cococcioni, et al., Advanced capabilities for materials modelling with quantum espresso, *Journal of Physics: Condensed Matter* 29 (46) (2017) 465901.
- [30] H. O. Rashid, N. R. Abdullah, V. Gudmundsson, Silicon on a graphene nanosheet with triangle- and dot-shape: Electronic structure, specific heat, and thermal conductivity from first-principle calculations, *Results in Physics* 15 (2019) 102625. doi:[10.1016/j.rinp.2019.102625](https://doi.org/10.1016/j.rinp.2019.102625).
URL <http://www.sciencedirect.com/science/article/pii/S2211379719317140>
- [31] A. Kokalj, Xcrysden—a new program for displaying crystalline structures and electron densities, *Journal of Molecular Graphics and Modelling* 17 (3) (1999) 176–179. doi:[10.1016/S1093-3263\(99\)00028-5](https://doi.org/10.1016/S1093-3263(99)00028-5).
URL <http://www.sciencedirect.com/science/article/pii/S1093326399000285>
- [32] N. R. Abdullah, Optical control of spin-dependent thermal transport in a quantum ring, *Physics Letters A* 382 (21) (2018) 1432–1436. doi:[10.1016/j.physleta.2018.03.042](https://doi.org/10.1016/j.physleta.2018.03.042).
URL <http://www.sciencedirect.com/science/article/pii/S0375960118303177>
- [33] G. K. Madsen, D. J. Singh, Boltztrap, a code for calculating band-structure dependent quantities, *Computer Physics Communications* 175 (1) (2006) 67–71.
- [34] N. R. Abdullah, H. O. Rashid, C.-S. Tang, A. Manolescu, V. Gudmundsson, Modeling electronic, mechanical, optical and thermal properties of graphene-like bc₆n materials: Role of prominent bn-bonds, *Physics Letters A* 384 (32) (2020) 126807. doi:<https://doi.org/10.1016/j.physleta.2020.126807>.
URL <http://www.sciencedirect.com/science/article/pii/S0375960120306745>
- [35] A. H. Castro Neto, F. Guinea, N. M. R. Peres, K. S. Novoselov, A. K. Geim, The electronic properties of graphene, *Rev. Mod. Phys.* 81 (2009) 109–162. doi:[10.1103/RevModPhys.81.109](https://doi.org/10.1103/RevModPhys.81.109).
URL <https://link.aps.org/doi/10.1103/RevModPhys.81.109>
- [36] N. R. Abdullah, H. O. Rashid, M. T. Kareem, C.-S. Tang, A. Manolescu, V. Gudmundsson, Effects of bonded and non-bonded b/n codoping of graphene on its stability, interaction energy, electronic structure, and power factor, *Physics Letters A* 384 (12) (2020) 126350. doi:[10.1016/j.physleta.2020.126350](https://doi.org/10.1016/j.physleta.2020.126350).
URL <http://www.sciencedirect.com/science/article/pii/S0375960120301602>
- [37] M. Alattas, U. Schwingenschlögl, Band gap control in bilayer graphene by co-doping with b-n pairs, *Scientific Reports* 8 (1) (2018) 17689. doi:[10.1038/s41598-018-35671-2](https://doi.org/10.1038/s41598-018-35671-2).
URL <https://doi.org/10.1038/s41598-018-35671-2>
- [38] G. Gómez-Santos, Thermal van der waals interaction between graphene layers, *Phys. Rev. B* 80 (2009) 245424. doi:[10.1103/PhysRevB.80.245424](https://doi.org/10.1103/PhysRevB.80.245424).
URL <https://link.aps.org/doi/10.1103/PhysRevB.80.245424>
- [39] L. A. Girifalco, M. Hodak, R. S. Lee, Carbon nanotubes, buckyballs, ropes, and a universal graphitic potential, *Phys. Rev. B* 62 (2000) 13104–13110. doi:[10.1103/PhysRevB.62.13104](https://doi.org/10.1103/PhysRevB.62.13104).
URL <https://link.aps.org/doi/10.1103/PhysRevB.62.13104>
- [40] N. R. Abdullah, C.-S. Tang, A. Manolescu, V. Gudmundsson, The interplay of electron-photon and cavity-environment coupling on the electron transport through a quantum dot system, *Physica E: Low-dimensional Systems and Nanostructures* 119 (2020) 113996. doi:<https://doi.org/10.1016/j.physe.2020.113996>.
URL <http://www.sciencedirect.com/science/article/pii/S1386947719312445>
- [41] A. Rajabpour, S. M. Vaez Allaei, Tuning thermal conductivity of bilayer graphene by inter-layer sp³ bonding: A molecular dynamics study, *Applied Physics Letters* 101 (5) (2012) 053115. arXiv:<https://doi.org/10.1063/1.4740259>, doi:[10.1063/1.4740259](https://doi.org/10.1063/1.4740259).
URL <https://doi.org/10.1063/1.4740259>
- [42] J. Berashevich, T. Chakraborty, On the nature of inter-layer interactions in a system of two graphene fragments, *The Journal of Physical Chemistry C* 115 (50) (2011) 24666–24673. arXiv:<https://doi.org/10.1021/jp2095032>, doi:[10.1021/jp2095032](https://doi.org/10.1021/jp2095032).
URL <https://doi.org/10.1021/jp2095032>
- [43] N. Al-Aqtash, K. M. Al-Tarawneh, T. Tawalbeh, I. Vasiliev, Ab initio study of the interactions between boron and nitrogen dopants in graphene, *Journal of Applied Physics* 112 (3) (2012) 034304. arXiv:<https://doi.org/10.1063/1.4742063>, doi:[10.1063/1.4742063](https://doi.org/10.1063/1.4742063).
URL <https://doi.org/10.1063/1.4742063>
- [44] P. Rani, G. S. Dubey, V. Jindal, Dft study of optical properties of pure and doped graphene, *Physica E: Low-dimensional Systems and Nanostructures* 62 (2014) 28–35. doi:[10.1016/j.physe.2014.04.010](https://doi.org/10.1016/j.physe.2014.04.010).
URL <http://www.sciencedirect.com/science/article/pii/S1386947714001374>
- [45] N. R. Abdullah, H. O. Rashid, C.-S. Tang, A. Manolescu, V. Gudmundsson, Properties of bsi₆n monolayers derived by first-principle computation, *Physica E: Low-dimensional Systems and Nanostructures* (2020) 114556. doi:<https://doi.org/10.1016/j.physe.2020.114556>.
URL <http://www.sciencedirect.com/science/article/pii/S1386947720316246>
- [46] M. L. Ould NE, M. Boujnah, A. Benyoussef, A. E. Kenz, Electronic and electrical conductivity of ab and aa-stacked bilayer graphene with tunable layer separation, *Journal of Superconductivity and Novel Magnetism* 30 (5) (2017) 1263–1267. doi:[10.1007/s10948-016-3910-7](https://doi.org/10.1007/s10948-016-3910-7).
URL <https://doi.org/10.1007/s10948-016-3910-7>
- [47] K. S. Kim, A. L. Walter, L. Moreschini, T. Seyller, K. Horn, E. Rotenberg, A. Bostwick, Coexisting massive and massless dirac fermions in symmetry-broken bilayer graphene, *Nature Materials* 12 (10) (2013) 887–892. doi:[10.1038/nmat3717](https://doi.org/10.1038/nmat3717).
URL <https://doi.org/10.1038/nmat3717>
- [48] X. Peng, R. Ahuja, Symmetry breaking induced bandgap in epitaxial graphene layers on sic, *Nano Letters* 8 (12) (2008) 4464–4468, pMID: 18959447. arXiv:<https://doi.org/10.1021/nl802409q>, doi:[10.1021/nl802409q](https://doi.org/10.1021/nl802409q).
URL <https://doi.org/10.1021/nl802409q>
- [49] N. R. Abdullah, H. O. Rashid, A. Manolescu, V. Gudmunds-

- son, Interlayer interaction controlling the properties of ab- and aa-stacked bilayer graphene-like bc14n and si2c14, *Surfaces and Interfaces* 21 (2020) 100740. doi:<https://doi.org/10.1016/j.surfin.2020.100740>.
URL <http://www.sciencedirect.com/science/article/pii/S246802302030732X>
- [50] B. Mohan, A. Kumar, P. Ahluwalia, A first principle study of interband transitions and electron energy loss in mono and bilayer graphene: Effect of external electric field, *Physica E: Low-dimensional Systems and Nanostructures* 44 (7) (2012) 1670 – 1674. doi:<https://doi.org/10.1016/j.physe.2012.04.017>.
URL <http://www.sciencedirect.com/science/article/pii/S1386947712001634>
- [51] N. R. Abdullah, C.-S. Tang, A. Manolescu, V. Gudmundsson, Thermoelectric inversion in a resonant quantum dot-cavity system in the steady-state regime, *Nanomaterials* 9 (5) (2019) 741.
- [52] B. Mortazavi, O. Rahaman, M. Makaremi, A. Dianat, G. Cuniberti, T. Rabczuk, First-principles investigation of mechanical properties of silicene, germanene and stanene, *Physica E: Low-dimensional Systems and Nanostructures* 87 (2017) 228 – 232. doi:<https://doi.org/10.1016/j.physe.2016.10.047>.
URL <http://www.sciencedirect.com/science/article/pii/S1386947716305690>
- [53] H. Nozaki, S. Itoh, Structural stability of bc2n, *Journal of Physics and Chemistry of Solids* 57 (1) (1996) 41 – 49. doi:[https://doi.org/10.1016/0022-3697\(95\)00088-7](https://doi.org/10.1016/0022-3697(95)00088-7).
URL <http://www.sciencedirect.com/science/article/pii/0022369795000887>
- [54] S. Bhandary, B. Sanyal, Graphene-boron nitride composite: A material with advanced functionalities, 2012.
- [55] A. Liu, Q. Peng, A molecular dynamics study of the mechanical properties of twisted bilayer graphene, *Micromachines* 9 (9) (2018) 440.
- [56] C. Lee, X. Wei, J. W. Kysar, J. Hone, Measurement of the elastic properties and intrinsic strength of monolayer graphene, *Science* 321 (5887) (2008) 385–388. arXiv:<https://science.sciencemag.org/content/321/5887/385.full.pdf>, doi:10.1126/science.1157996.
URL <https://science.sciencemag.org/content/321/5887/385>
- [57] S. Yiğen, V. Tayari, J. O. Island, J. M. Porter, A. R. Champagne, Electronic thermal conductivity measurements in intrinsic graphene, *Phys. Rev. B* 87 (2013) 241411. doi:10.1103/PhysRevB.87.241411.
URL <https://link.aps.org/doi/10.1103/PhysRevB.87.241411>
- [58] H. Sadeghi, S. Sangtarash, C. J. Lambert, Enhanced thermoelectric efficiency of porous silicene nanoribbons, *Scientific Reports* 5 (1) (2015) 9514. doi:10.1038/srep09514.
URL <https://doi.org/10.1038/srep09514>
- [59] N. R. Abdullah, G. A. Mohammed, H. O. Rashid, V. Gudmundsson, Electronic, thermal, and optical properties of graphene like sixx structures: Significant effects of si atom configurations, *Physics Letters A* 384 (24) (2020) 126578. doi:<https://doi.org/10.1016/j.physleta.2020.126578>.
URL <http://www.sciencedirect.com/science/article/pii/S037596012030445X>
- [60] R. Pilemalm, S. Simak, P. Eklund, The effect of point defects on the electronic density of states of scm_n2-type (m= v, nb, ta) phases, *Condensed Matter* 4 (3) (2019) 70.
- [61] N. R. Abdullah, R. B. Marif, H. O. Rashid, Photon-mediated thermoelectric and heat currents through a resonant quantum wire-cavity system, *Energies* 12 (6) (2019) 1082.
- [62] F. Bonaccorso, Z. Sun, T. Hasan, A. C. Ferrari, Graphene photonics and optoelectronics, *Nature Photonics* 4 (9) (2010) 611–622. doi:10.1038/nphoton.2010.186.
URL <https://doi.org/10.1038/nphoton.2010.186>
- [63] B.-L. Huang, C.-P. Chuu, M.-F. Lin, Asymmetry-enriched electronic and optical properties of bilayer graphene, *Scientific Reports* 9 (1) (2019) 859. doi:10.1038/s41598-018-37058-9.
URL <https://doi.org/10.1038/s41598-018-37058-9>
- [64] N. R. Abdullah, V. Gudmundsson, Single-photon controlled thermospin transport in a resonant ring-cavity system, *Physica E: Low-dimensional Systems and Nanostructures* 104 (2018) 223–228. doi:10.1016/j.physe.2018.07.036.
URL <http://www.sciencedirect.com/science/article/pii/S1386947718301838>
- [65] P. Nath, D. Sanyal, D. Jana, Ab-initio calculation of optical properties of aa-stacked bilayer graphene with tunable layer separation, *Current Applied Physics* 15 (6) (2015) 691 – 697. doi:<https://doi.org/10.1016/j.cap.2015.03.011>.
URL <http://www.sciencedirect.com/science/article/pii/S1567173915000887>
- [66] N. R. Abdullah, C.-S. Tang, A. Manolescu, V. Gudmundsson, Cavity-photon-switched coherent transient transport in a double quantum waveguide, *Journal of Applied Physics* 116 (23) (2014) 233104. arXiv:<https://doi.org/10.1063/1.4904907>, doi:10.1063/1.4904907.
URL <https://doi.org/10.1063/1.4904907>
- [67] N. R. Abdullah, A. H. Fatah, J. M. A. Fatah, Effects of magnetic field on photon-induced quantum transport in a single dot-cavity system, *Chinese Physics B* 25 (11) (2016) 114206.
URL <http://stacks.iop.org/1674-1056/25/i=11/a=114206>